SUPPLEMENTAL MATERIAL

Human Atrial Fibrillation Drivers Correlated with Integrated Functional and Structural Imaging to Benefit Clinical Mapping

Hansen et al.: Validation of Reentrant AF Drivers

Authors: Brian J. Hansen, BSc[a,b], Jichao Zhao, PhD[c], Ning Li, MD, PhD[a.b], Alexander Zolotarev, BSc[a,d], Stanislav Zakharkin, PhD[a], Yufeng Wang, BSc[c], Josh Atwal[c], Anuradha Kalyanasundaram, PhD[a,b], Suhaib H. Abudulwahed[a], Katelynn M. Helfrich, BSc[a], Anna Bratasz, PhD[b], Kimerly A. Powell, PhD[b], Bryan Whitson, MD[b,e], Peter J. Mohler, PhD[b,f], Paul ML. Janssen, PhD[a,b], Orlando P. Simonetti, PhD[b,g], John D. Hummel, MD[b,f], Vadim V. Fedorov, PhD[a,b]

Affiliations: [a]Department of Physiology & Cell Biology; [b]Davis Heart & Lung Research Institute The Ohio State University Wexner Medical Center, Columbus, OH, USA.; [c]Auckland Bioengineering Institute, The University of Auckland, Auckland, New Zealand; [d]Moscow Institute of Physic and Technology, Dolgoprudny, Russian Federation; [e]Department of Surgery; [f]Department of Internal Medicine; [g]Department of Biomedical Engineering, The Ohio State University Wexner Medical Center, Columbus, OH, USA.

Address for correspondence: Vadim V. Fedorov, PhD

Department of Physiology and Cell Biology, The Ohio State University Wexner Medical Center

5196 Graves Hall, 333 W 10th Ave, Columbus OH 43210-1218

tel: 1-614-293-3706 fax: 1-614-292-4888

e-mail: vadim.fedorov@osumc.edu

Supplemental Methods

Explanted Human Hearts and Inclusion criteria

This study was approved by The Ohio State University Institutional Review Board, which granted exemption for informed consent. De-identified, coded human hearts were obtained from The Ohio State University Cardiac Transplant Team and LifeLine of Ohio Organ Procurement Organization. Due to the focus of the study, only atrial preparations with sustained AF (>1min) and localized drivers confirmed by NIOM were included in this study's driver analysis (n=11). The current study presents entirely new analyses and techniques, such as integrated phase singularity density, FIRM multielectrode mapping, and 3D CE-MRI fibrosis analysis, which were not previously published in a subset of hearts included in other studies.(1-3) Patient-specific data and the methods used to study each heart are presented in **Online Table 1**.

Near-Infrared Optical Mapping of Coronary-Perfused Human Atrial Preparations

All human hearts (n=11) were obtained in the operating room at the time of cross-clamp and immediately preserved with cold cardioplegic solution (1–3°C). Hearts were transported to the experimental lab within 15 minutes and coronary-perfused with oxygenated cardioplegic solution at 4°C to prevent any potential tissue degradation. Human whole intact atrial (n=2), lateral RA (n=8), and a lateral left atrium were isolated and coronary-perfused with oxygenated Tyrode solution at constant pressure (50–60 mm Hg) and temperature (37°C) as previously described.(2,3) Whole intact atrial preparations included the entire left and right atrial walls, entire atrioventricular groove, >2mm of each pulmonary vein, and >3mm of the superior vena cava, but were cut at the junction of the inferior vena cava and right atrium for liver transplant. The right atria preparations included the lateral right atrial free wall bordered by the right aspect

of Bachmann's bundle superiorly, the inferior vena cava inferiorly, the junction of the pectinate muscles with the crista terminalis medially, and a thin portion of the right ventricle laterally. These preparations included the right atrial appendage. The left atrial preparation #514489 included the lateral left atrial free wall bordered by the left aspect of Bachmann's bundle superiorly, the coronary sinus inferiorly, the posterior left atria medially, and a thin portion of the left ventricle laterally. This preparation included the left pulmonary veins and the left atrial appendage. Each preparation contained an intact, long section of the right and/or left coronary artery along its atrioventricular groove, which was cannulated with a flexible plastic cannula (diameter 2 mm), custom-made for these experiments. All arterial leaks in the preparations were ligated with silk suture. All mapped preparations excluded regions of poor coronary perfusion/ischemia.

After 40-70 minutes of washout with oxygenated Tyrode's solution and warming to 37°C to ensure tissue recovery and stabilization, the human atrial preparations were immobilized with 10μM blebbistatin and stained with near-infrared dye di-4-ANBDQBS (10-40μM).(2,3) The preparations and all recording electrodes were fully immersed in the perfusion efflux, which assured appropriate superfusion and reliable signal collection. Imaging was simultaneously conducted with 2-4 MiCAM Ultima-L CMOS cameras (SciMedia, Ltd., CA) from atrial epicardial and endocardial (**Online Figure 1**) fields of view (from 3.3x3.3mm^2-9.4x9.4mm^2, 100×100 pixel resolution). A pseudo atrial electrocardiogram was recorded by Ag-Cl electrodes, and a 7F 4mm-tip quadripolar ablation catheter recorded local bipolar electrograms. Data were analyzed using a customized Matlab (MathWorks) program as previously described.(3) Conduction and repolarization were assessed at 500ms cycle length (CL) pacing. Burst pacing

was used to test AF inducibility at baseline and after pharmacologic stimulation. If sustained AF was not inducible at baseline, pharmacologic stimulation by isoproterenol (10nM), adenosine (100μM), or pinacidil (20-100μM), was used to induce sustained AF as previously described.(2-4) These drugs produce the action potential shortening that would be expected in fibrillating human atria in-vivo, where autonomic stimulation and metabolic stresses are present.(4,5)

At baseline, all human atrial preparations were either in sinus rhythm or paced at 500ms CL if no sinoatrial node was present. Moreover, all hearts showed conduction and repolarization parameters within clinically reported ranges for diseased human hearts and did not include ischemic tissue, as we previously validated.(2,3)

NIOM-defined AF Driver and Non-Driver Regions

Dominant frequency (DF) was analyzed across the tissue using Fast Fourier Transform as previously described.(3) Activation maps created from the maximum upstroke (dV/dt max) of the optical action potentials (OAPs, Figure 1A) within areas of highest DF were used to identify repetitive sources of activation and defined as AF drivers, as done previously.(3) These drivers were temporally stable for >70% of AF duration when there was only 1 driver, or >30% if 2 drivers were present. Temporal stability of AF drivers was calculated as the percent of activation cycles with activation originating within a driver region during 8s recording.(2) Based on the average size of intramural reentrant AF drivers seen previously,(2,3) AF driver regions were limited to a 1x2cm^2 area of the atrial surface for regional analyses of functional and structural characteristics. Neighboring non-driver regions, also 1x2cm^2, were selected for comparative statistical analysis (**Figure 1C**).

Activation patterns in AF driver regions were classified into two categories: (1) reentrant patterns, with pivot points where conduction makes a U-turn; (2) breakthrough patterns, with focal activation consistently emanating from a driver region, seen by dual-sided NIOM to be caused by intramural reentry (**Online Figure 2**).(2)

Hilbert Transform of OAPs performed by pseudo-empirical mode decomposition was used to calculate the local phase.(6,7) PSs, representing the center of wavefront rotation, were calculated for every pixel in every time frame using a convolution method(7) by sampling neighboring pixels within a 9-pixel diameter area, to reduce the amount of false-positive PSs caused by wavebreaks.(8) PS density (PSD) was calculated for each pixel as the percent of total temporal frames during 8s recordings (**Figure 1B**).

Integration of Focal Impulse and Rotor Mapping

To directly compare NIOM and clinical multi-electrode mapping, two standard 64-electrode (8x8) FIRMap catheters (Abbott Labs, Chicago, IL) were customized and flattened out into panoramic catheters with a resolution of ~9x9mm^2 (Online Figure 1). The flattened catheters were directly placed on the epicardial and endocardial lateral RA surfaces. Instead of an endocardial flat catheter for the intact atria of Heart 402879, two endocardial FIRMap basket catheters were inserted through the inferior vena cava and interatrial septum to recapitulate clinical mapping. However, since no direct spatial correlation with NIOM could be performed in these settings, the data obtained are not presented here.(9) RhythmView 6.1 (Abbott Labs, Chicago, IL) processed AF activation patterns. Due to restrictions within RhythmView at AF CL

<120ms, autonomous activation analysis could often skip every other beat. Blinded to NIOM and structural data, electrogram activation times for a 4s FIRM epoch within NIOM recordings were marked manually on the unipolar signals by Abbott engineers in accordance with the RhythmView criteria. The autonomous Rotational Activity Profile (RAP) marked by RhythmView 6.1, which combines unipolar electrogram derived PSD and activation, was used to define reentrant patterns of AF drivers by FIRM.(10) Focal driver patterns were defined as activation beginning at 1 electrode or as a group of neighboring electrodes activating simultaneously and spreading outward. The location of a driver was congruent between NIOM and FIRM if the location differed by ≤1 inter-electrode distance. RAP locations not matched with a NIOM-defined AF driver were considered false-positives. For electrogram DF analysis, each unipolar atrial electrogram from the catheter was resampled to 1 kHz and processed by a bandpass Butterworth filter of order 4 with a lower cutoff frequency of 0.5 Hz and higher cutoff frequency 30 Hz. Then the resultant signals were further filtered by a Zero-phase digital filtering in both the forward and reverse directions. Then the DF was estimated using a Fast Fourier Transform.

Targeted Ablation

During sustained AF, a radiofrequency generator was used to apply 75W energy for 60s through the 8mm-tip 7F ablation catheter at NIOM-defined AF driver locations in order to produce transmural ablation lesions (~6.5x3.7mm^2). Termination of AF or conversion of AF to atrial tachycardia by the targeted ablation were all used to confirm NIOM-defined AF drivers as the mechanism of sustained AF.(11) Ablation lesions were split into three categories: untargeted ablation, which was outside the driver region and had no acute effect on AF pattern or stability;

targeted ablation, which slowed AF cycle lengths by >10%, converted AF to organized atrial tachycardia, or terminated AF; and tachycardia ablation, which was used to terminate post-ablation atrial tachycardia and prevent the reinduction of arrhythmia.

Contrast-Enhanced Magnetic Resonance Imaging

Gadolinium-based CE-MRI imaged at ~95x95x95μm^3 to 180x180x360μm^3 resolution with a 9.4T Bruker BioSpin Spectrometer (Ettlingen, Germany) was used to define atrial anatomy (**Online Figure 1**) and the 3D distribution of fibrosis, as previously described.(1) 3D human atria were segmented and then interpolated to an isotropic resolution using a custom Matlab program (MathWorks).(1) Optical maps and 3D human atrial reconstructions were reconciled using anatomical landmarks. Fibrosis was identified based on signal intensity thresholds defined by matching fibrosis percent in resliced 2D CE-MRI sections with corresponding sections of Masson's Trichrome histology staining (**Figure 6B**).(1,3,12) To determine the volume of the atrial wall, Laplace's equation bounded by the epicardial and endocardial surfaces was solved to obtain numerical values at each pixel within the 3D atria, smoothly varying from one surface to the other.(1) These values were used to divide the 3D atrial tissue into three sub-volumes: sub-epicardium, intramural wall, and sub-endocardium (**Figure 6B**). CE-MRI-detected fibrosis is reported as the percent of gadolinium-enhanced voxels within the sub-volume of the atrial wall.

Online Table 1. *Human heart information*

Heart ID	Age	Sex	Prep	Diagnoses
947200 (1,13)	63	F	Whole Atria	AF in OR, HTN
380071 (3)	43	F	RA	CAD, HTN, DM, COPD, Obesity
514955 (3)	67	F	RA	ICM, CAD, DM, PM/ICD, LVAD
203056 (3)	51	M	RA	NICM, PM/ICD, LVAD
879242 (3)	58	F	RA	Persistent AF, NICM, PM/ICD
402879 (2)	54	M	Whole Atria	HTN
645444 (2)	47	M	RA	ICM, CAD, HTN, DM, LVAD
728878 (2)	40	M	RA	NICM, PM/ICD, LVAD
963542 (2)	60	F	RA	NICM, PM/ICD
497522	62	F	RA	NICM, PM/ICD
514489	42	F	LA	MI, COPD

Abbreviations: AF- atrial fibrillation; CAD-coronary artery disease; COPD-chronic obstructive pulmonary disease; DM-diabetes mellitus; HTN-hypertension; ICM-ischemic cardiomyopathy; LA-left atrium; LVAD-left ventricular assist device; MI-myocardial infarction; NICM-non-ischemic cardiomyopathy; OR-operating room; PM/ICD-pacemaker/implantable cardiac defibrillator; RA- right atrium.

Online Table 2. *Procedures and surfaces mapped for each atrial preparation*

Heart ID	Prep	Optical Mapping Surface	FIRM Placement	CE-MRI	Ablation (Endo)
947200	Whole Atria	Epi		X	
380071	RA	Epi/Endo		X	X
514955	RA	Epi/Endo		X	X
203056	RA	Epi/Endo		X	X
879242	RA	Epi/Endo		X	X
402879	Whole Atria	Epi	Epi/BC	X	
645444	RA	Epi/Endo	Epi/Endo	X	X
728878	RA	Epi/Endo	Epi/Endo	X	X
963542	RA	Epi/Endo	Epi/Endo	X	X
497522	RA	Epi/Endo	Epi/Endo	X	
514489	LA	Epi/Endo	Endo	X	X

Abbreviations: BC- FIRM basket catheter; CE-MRI- contrast-enhanced magnetic resonance imaging; Endo/Epi- Endocardial/Epicardial mapping; FIRM-Focal Impulse and Rotor Mapping; LA-left atrium; RA- right atrium.

Online Table 3. *Characteristics of Atrial Fibrillation Drivers in Human Atria*

					DF (Hz)		Visualization Pattern			
Heart ID	Episode/ Condition	Surface	Driver	Temporal Stability	NIOM	FIRM	NIOM	FIRM	Location Match	# False-Positives
402879	Baseline	Epi	1	79%	6.6	6.6	Breakthrough	No Driver	No	0
	Ado 100µM	Epi	2	74%	13.43	13.42	Reentry	Reentry	Yes	2
			3	33%	13.31	13.18	Reentry	Reentry	Yes	
645444	Pina 40µM	Endo	1	100%	8.55	8.3	Breakthrough	No Driver	No	0
		Epi	1	100%	8.55	8.3	Breakthrough	Breakthrough	Yes	0
Post-RFA	Pina 40µM	Endo	2	100%	11.73	11.78	Reentry	Reentry	Yes	2
		Epi	2	100%	11.73	11.78	Breakthrough	Breakthrough	Yes	1
728878	Pina 20µM	Endo	1	100%	12.21	12.08	Reentry	No Driver	No	1
			2	100%	12.34	12.33	Reentry	Reentry	Yes	
		Epi	1	97%	12.34	12.33	Reentry	No Driver	No	0
			2	98%	12.21	12.08	Breakthrough	Breakthrough	Yes	
Post-RFA	Pina 20µM,	Endo	3	100%	9.65	8.06	Reentry	Reentry	Yes	1
		Epi	3	100%	9.65	8.06	Reentry	Breakthrough	Yes	1
963542	Pina 100µM	Endo	1	100%	11.6	11.84	Reentry	Reentry	Yes	2
		Epi	1	100%	11.6	11.78	Breakthrough	Breakthrough	Yes	2
497522	Pina 30µM	Endo	1	100%	9.77	9.64	Reentry	Reentry	Yes	3
		Epi	1	100%	9.77	9.64	Reentry	Breakthrough	Yes	1
	Pina 50µM	Endo	2	100%	10.01	9.89	Reentry	Reentry	Yes	1
		Epi	2	100%	10.01	9.89	Reentry	Reentry	Yes	1
514489 Post-RFA	Pina 30µM	Endo	1	100%	6.7	6.67	Reentry	Reentry	Yes	0
		Epi	1	100%	6.7		Reentry			
947200	Iso 10nM	Epi	1	100%	7.57		Reentry			
			2	43%	7.57		Reentry			
	Iso 10nM	Epi	3	100%	4.27		Reentry			
380071	Pina 100µM	Endo	1	100%	7.7		Reentry			
		Epi	1	100%	7.7		Breakthrough			
514955	Pina 100µM	Endo	1	100%	15.53		Reentry			
		Epi	1	100%	15.44		Breakthrough			
203056	Pina 40µM	Endo	1	100%	9.09		Reentry			
		Epi	1	100%	9.09		Breakthrough			
879242	Pina 30µM	Endo	1	100%	4.79		Reentry			
		Epi	1	100%	4.79		Breakthrough			
Post-RFA	Pina 30µM	Endo	2	100%	3.32		Reentry			
		Epi	2	100%	3.32		Reentry			

Abbreviations: Ado-adenosine; DF-dominant frequency; Endo-endocardium; Epi-epicardium; FIRM- Focal Impulse and Rotor Mapping; Iso-isoproterenol; NIOM-near-infrared optical mapping; Pina-pinacidil; RFA-radiofrequency ablation. Red font highlights discordant endocardial mapping while blue font highlights discordant epicardial mapping.

Supplemental Figures

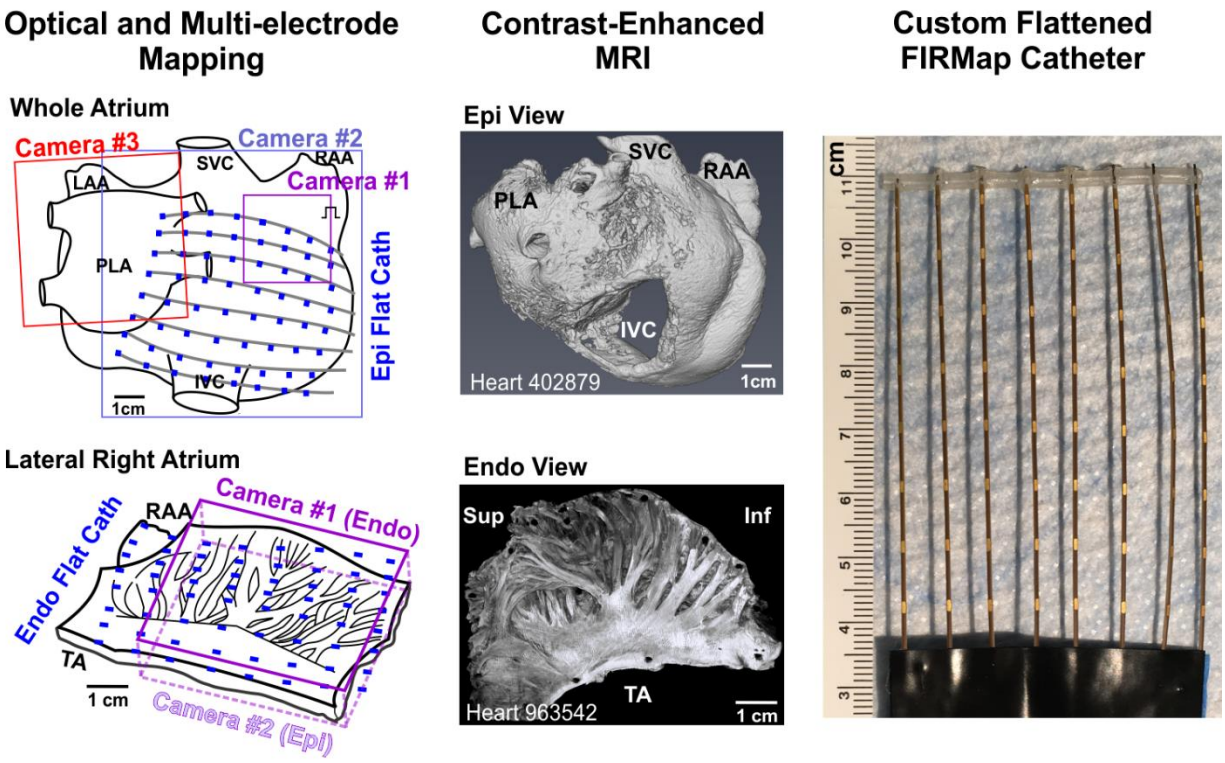

Online Figure 1. *Integrated Functional and Structural Mapping*. Left, Schematics showing optical fields of view for each camera and the placement of the customized flattened FIRMap catheters for the whole intact preparations (Top), which include both left and right atria mapped from the epicardium (epi), and the lateral right atrial preparations (Bottom), which were mapped simultaneously from both epi and endocardium (endo). Center, 3D contrast-enhanced MRI reconstructed from high-resolution 2D sections. Left, photo of custom flattened FIRMap catheter. Inf/Sup-inferior/superior lateral right atrium (LRA); IVC/SVC-inferior/superior vena cava; LAA/RAA-left/right atrial appendage; PLA-posterior left atrium; TA-tricuspid annulus.

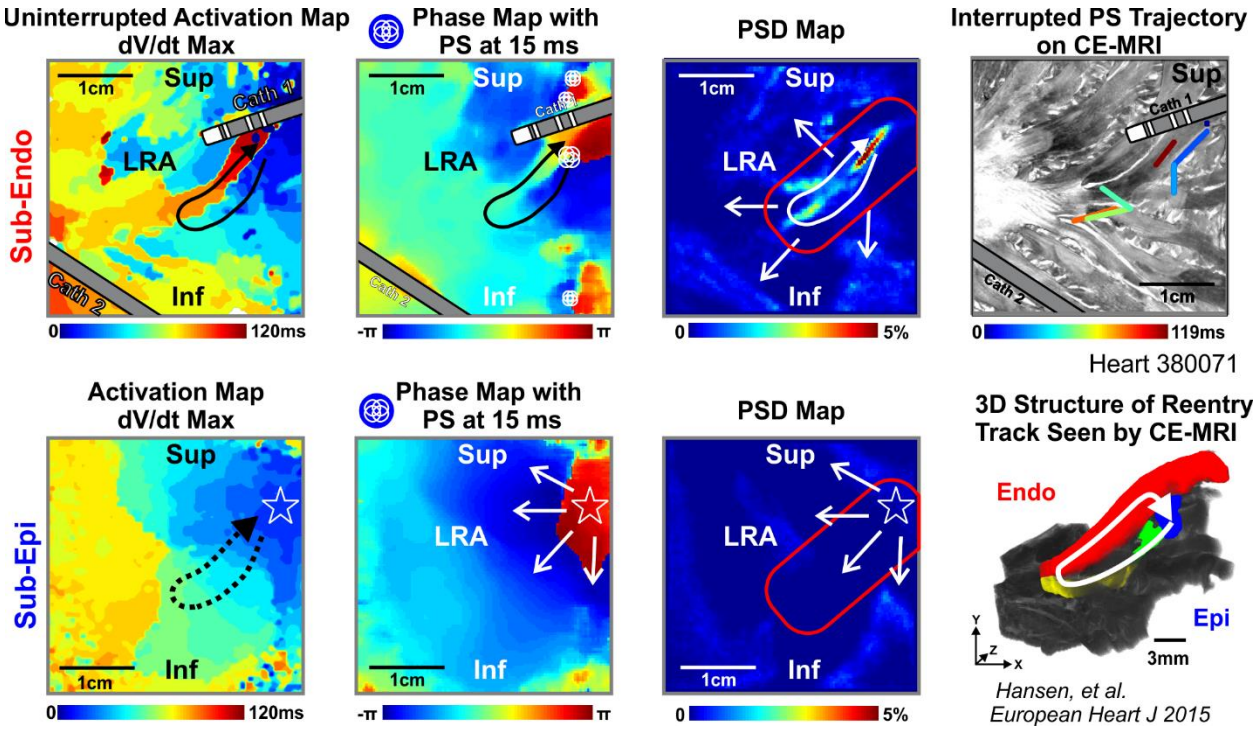

Online Figure 2. *Phase Singularity Density Analysis of Dual-sided Near-Infrared Optical Mapping* (NIOM) *During Sustained AF*. All data from Heart 380071 LRA. Left to Right, NIOM activation maps, snapshots of instantaneous phase at the frame 15 of the activation maps with phase singularities (PS) shown by white circles; NIOM phase singularity density (PSD) map showing the percent of frames in an 8-second recording that each pixel was labeled with a PS. Simultaneous dual-sided NIOM maps of an AF driver with a reentrant pattern seen from the sub-endocardium (sub-Endo, Top) and a breakthrough pattern (star) seen from the sub-epicardium (sub-Epi, Bottom). Top Right, tracing of a single PS as it drifted and intermittently disappeared and reappeared over one cycle of the reentrant driver overlaid on the 3D CE-MRI of the atrial wall mapped. Bottom Right, 3D reconstruction of the intramural microanatomic reentrant AF driver track with intramural bundles highlighted in yellow, green, and blue. 3D CE-MRI adapted from Hansen et al., *Euro Heart J* 2015.(3) Abbreviations as in Online Figure 1.

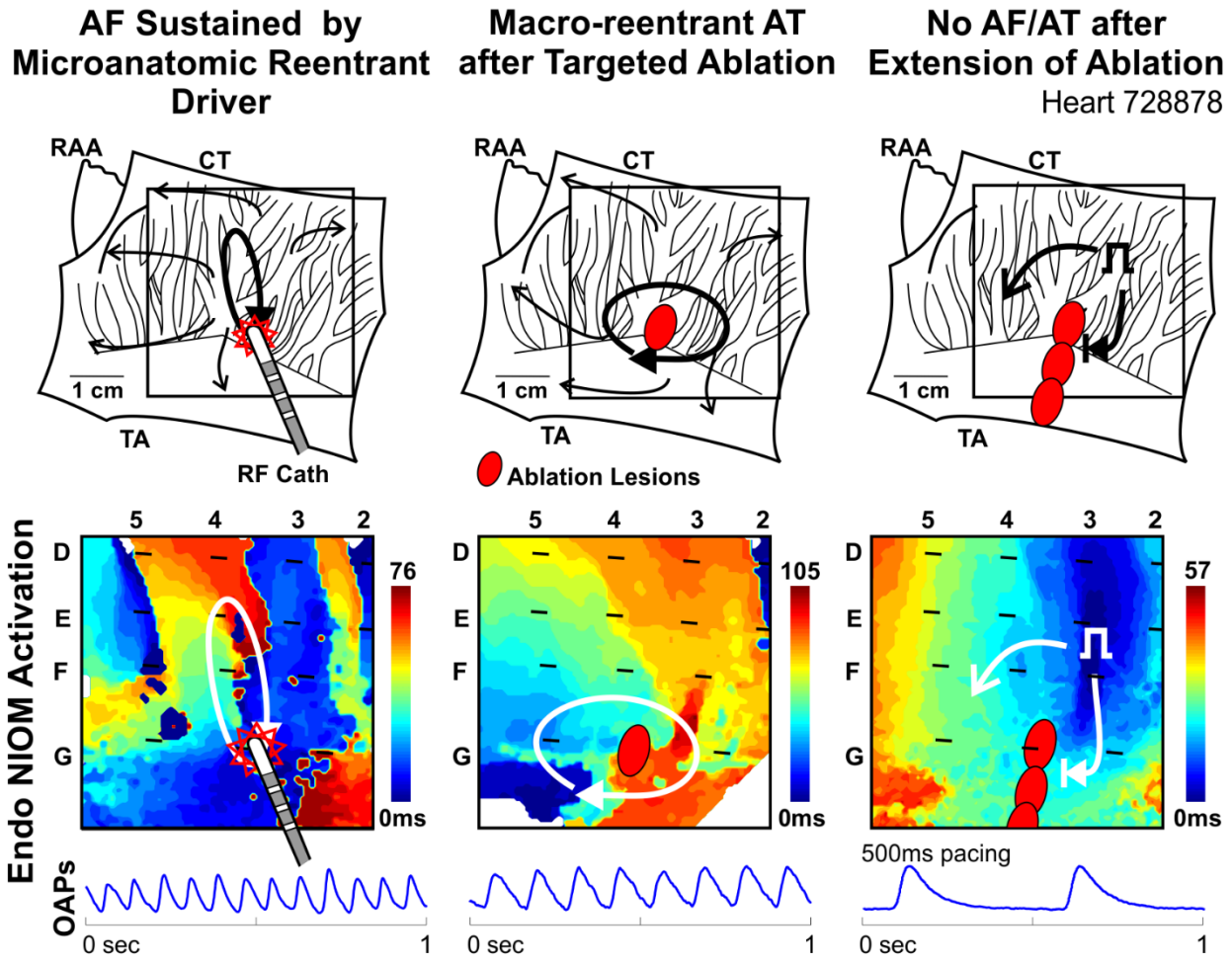

Online Figure 3. *Targeted Radiofrequency Ablation Verifies Reentrant Drivers of AF*. All data from Heart 728878. Schematics (Top) and NIOM activation maps (Bottom) showing a single radiofrequency (RF) ablation lesion on the track of the reentrant AF driver (Left) converted the AF to macro-reentrant atrial tachycardia (AT) around the ablation lesion (Middle). Subsequent ablation connecting the first lesion to the tricuspid annulus (TA) terminated the arrhythmia and prevented its reinduction (Right). Abbreviations as in Online Figure 1**.** CT-crista terminalis.

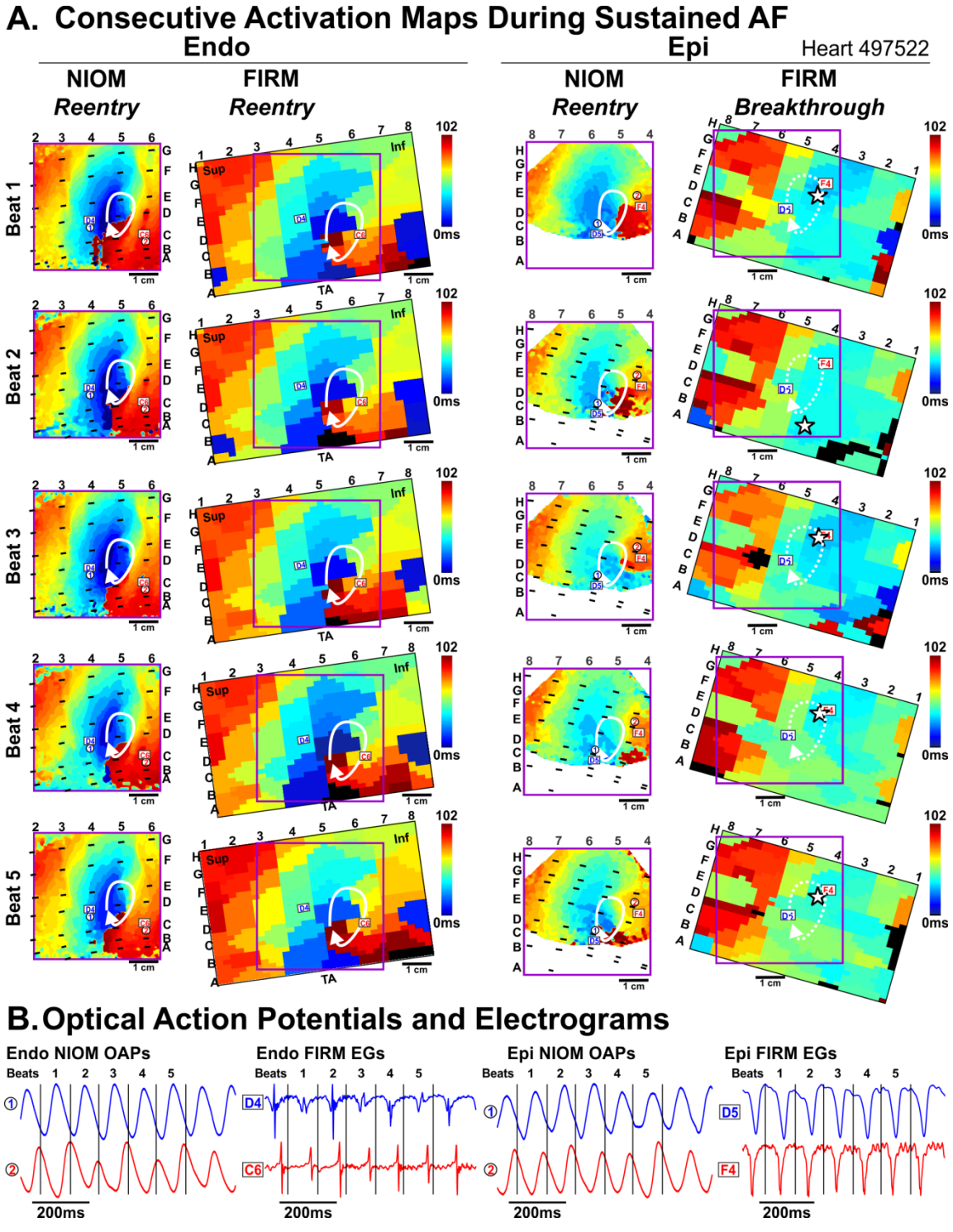

Online Figure 4. *Simultaneous Dual-sided Mapping by both NIOM and FIRM show Temporal Stability of Intramural Reentrant Driver.* All data from Heart 497522. **A**. Activation maps from five consecutive AF beats arranged in rows. From right to left: Endo NIOM activation maps,

Endo FIRM activation maps, Epi NIOM activation maps, Epi FIRM activation maps. Arrows show reentrant patterns, dotted arrow shows position of NIOM reentry on the FIRM map, and star shows earliest breakthrough location. **B**. Simultaneous Optical action potentials (OAPs) and unipolar electrograms (EGs) from the same time segment. Abbreviations as in Online Figure 1.

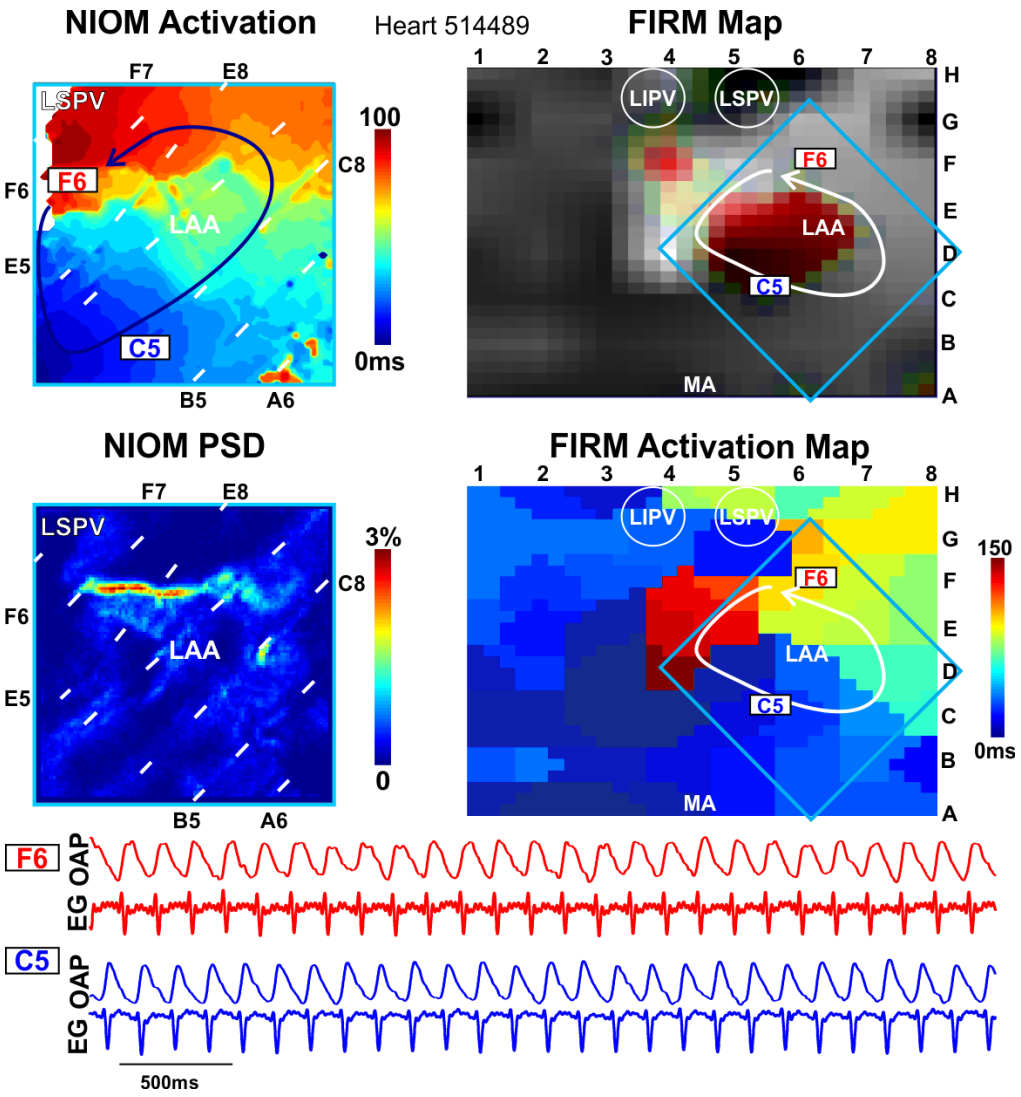

Online Figure 5. *Post-ablation AF Driver mapped simultaneously by Endocardial NIOM and Multi-Electrodes in the Left Atrium*. All data from Heart 514489. Left: Endocardial NIOM activation map (Top) and corresponding PSD map (Bottom). Right: snapshot of endocardial FIRM movie with rotation activity profile (RAP) (Top) and multi-electrode activation map (Bottom) highlighting the same reentrant path sustaining AF that was seen by NIOM. Abbreviations as in Online Figure 1; LAA-left atrial appendage; LIPV/LSPV-left inferior/superior pulmonary vein; MA-mitral annulus.

Supplemental Movies

Movie 1. Focal Impulse and Rotor Mapping (FIRM) activation movie from RhythmView 6.1 of an epicardial flat catheter recording during sustained AF in intact atria, Heart 402879. FIRM highlighted RAP at electrodes GH678 and CD56 which overlaid NIOM-defined reentrant AF drivers. This AF visualization is also shown in **Figures 1A&B** and **Figure 3**, but the movie needs to be rotated 180 degrees for comparison**.** Left box intentionally left blank.

Movie 2. FIRM activation movie from RhythmView 6.1 of simultaneous endocardial (Left Panel) and epicardial (Right Panel) flat catheter recordings during sustained AF in lateral right atrium, Heart 645444. Basket 1 (Right Panel) is from an epicardial flat catheter and shows a focal pattern. Basket 2 (Left Panel) is from an endocardial flat catheter and does not show any localized driver activity, while near-infrared optical mapping defined stable breakthrough pattern. Right Panel AF visualization is also shown in **Figure 4A**, but the movie needs to be mirrored over the y-axis for comparison.

Supplemental Reference List

1. Zhao J, Hansen BJ, Wang Y et al. 3D Integrated functional, structural, and computational mapping to define the structural "fingerprints" of heart-specific atrial fibrillation drivers in human heart ex-vivo. J Am Heart Assoc 2017;6(8):e005922.
2. Li N, Csepe TA, Hansen BJ et al. Adenosine-Induced Atrial Fibrillation: Localized Reentrant Drivers in Lateral Right Atria due to Heterogeneous Expression of Adenosine

A1 Receptors and GIRK4 Subunits in the Human Heart. Circulation 2016;134(6):486-498.

3. Hansen BJ, Zhao J, Csepe TA et al. Atrial fibrillation driven by micro-anatomic intramural re-entry revealed by simultaneous sub-epicardial and sub-endocardial optical mapping in explanted human hearts. Eur Heart J 2015;36(35):2390-2401.
4. Fedorov VV, Glukhov AV, Ambrosi CM et al. Effects of KATP channel openers diazoxide and pinacidil in coronary-perfused atria and ventricles from failing and non-failing human hearts. J Mol Cell Cardiol 2011;51(2):215-225.
5. Heijman J, Guichard JB, Dobrev D, Nattel S. Translational Challenges in Atrial Fibrillation. Circ Res 2018;122(5):752-773.
6. Yamazaki M, Mironov S, Taravant C et al. Heterogeneous atrial wall thickness and stretch promote scroll waves anchoring during atrial fibrillation. Cardiovasc Res 2012;94(1):48-57.
7. Bray MA, Wikswo JP. Considerations in phase plane analysis for nonstationary reentrant cardiac behavior. Phys Rev E Stat Nonlin Soft Matter Phys 2002;65(5 Pt 1):051902.
8. Kuklik P, Zeemering S, Maesen B et al. Reconstruction of instantaneous phase of unipolar atrial contact electrogram using a concept of sinusoidal recomposition and Hilbert transform. IEEE Trans Biomed Eng 2015;62(1):296-302.
9. Hansen BJ, Li N, Csepe TA et al. Intramural Drivers of Human Atrial Fibrillation Visualized Differently from the Endocardium and Epicardium by Simultaneous Dual-Sided Electrode and Optical Mapping. Heart Rhythm 2016;15(5):S115.

10. Alhusseini M, Vidmar D, Meckler GL et al. Two Independent Mapping Techniques Identify Rotational Activity Patterns at Sites of Local Termination During Persistent Atrial Fibrillation. J Cardiovasc Electrophysiol 2017;28(6):615-622.
11. Hansen BJ, Briggs C, Moore BT et al. Human atrial fibrillation drivers seen simultaneously by focal impulse and rotor mapping and highresolution optical mapping. Circulation 2015;132:A18402.
12. Csepe TA, Zhao J, Sul LV et al. Novel Application of 3D Contrast Enhanced CMR to Define Fibrotic Structure of the Human Sinoatrial Node *In-vivo* . Eur Heart J Cardiovasc Imaging 2017;18(8):862-869.
13. Zhao J, Hansen BJ, Csepe TA et al. Intergration of High-Resolution Optical Mapping and 3-Dimensional Micro-Computed Tomographic Imaging to Resolve the Structure Basis of Atrial Conduction in the Human Heart. Circulation Arrhythm Electrophysiol 2015;8:1514-1517.